Desalination and Water Treatment
www.deswater.com

doi:10.5004/dwt.2019.24038

153 (2019) 165–178
June

A new adsorbent modified from walnut shell for the adsorption of Ni(II) from aqueous solution

Shenmaishang Li, Minqian Qiu, Zuoxiang Zeng*, Weilan Xue

Institute of Chemical Engineering, East China University of Science and Technology, 200237 Shanghai, China, Phone: +86 021-64253081, email: zengzx@ecust.edu.cn (Z. Zeng)

Received 2 July 2018; Accepted 25 February 2019

ABSTRACT

A new adsorbent modified from walnut shell (MWNS) was prepared by grafting aspartic acid onto walnut shell (WNS). Two samples (MWNS1, MWNS2) were characterized through SEM, elemental analysis, XPS, point of zero charge analysis and N_2–BET analysis. The adsorption behaviors of Ni(II) onto WNS, MWNS1 and MWNS2 were studied. The results showed that the adsorption kinetics of Ni(II) onto MWNS1 and MWNS2 followed the pseudo-second-order model, while the ones onto WNS followed the pseudo-first-order model. The adsorption mechanism was investigated using the intraparticle diffusion model. The equilibrium data of Ni(II) adsorption onto MWNS2 were analyzed using the Langmuir, Freundlich and Dubinin–Redushkevich (D–R) models. Meanwhile, the mean feature concentration (C_e') correlated with temperature was determined. The values of the mean free energy (E) obtained from the D–R model indicated the adsorption process was conducted by monolayer chemisorption for $C_e<C_e'$ and followed by physical adsorption for $C_e>C_e'$. The thermodynamic parameters (ΔG, ΔH and ΔS) showed that the Ni(II) adsorption onto MWNS2 was spontaneous, endothermic and entropy driven. Recycling property of MWNS2 was studied.

Keywords: Walnut shell; Ni(II); Kinetics; Thermodynamics; Recycle

1. Introduction

The water pollution by the presence of metal ion is a widespread environmental problem for developing countries. The release of nickel (Ni) into aquatic ecosystems roots from various industries processes such as nickel–cadmium batteries, catalyst, electroplating, coinage, steel manufacturing, plastics manufacturing, porcelain enameling, fertilizers, pigment industries, mining and metallurgical industries [1,2]. The acceptable tolerance of nickel concentration is below 0.01 mg·L^{-1} and 2.0 mg·L^{-1} in drinking water and industrial effluent, respectively [3]. The Ni(II) concentration beyond permissible levels is seriously hazardous to human beings because of the intrinsic carcinogenic nature (lung cancer and nose cancer) [4], and will cause neurological disorder, skin dermatitis, kidney disease, etc [5,6]. Therefore, several physical and chemical methodologies have to be employed for Ni(II) removal, which includes chemical precipitation, electrolysis, reduction, biosorption, adsorption, ion exchange and membrane filtration [1,7,8]. However, most of these techniques have their own disadvantages such as partial efficiency, secondary pollution, high operational cost and sensitive operating conditions [9]. On the other hand, adsorption is recognized as a low-cost, effective and flexible method and could be used to remove metal ions from contaminated waters at low concentrations.

Nowadays, more and more researches focus on the application of low-cost and easily available adsorbents, especially the biomass which comes from waste agricultural materials such as rice bran [2], walnut, hazelnut and almond shell [10], wheat residue [11], mango kernel [12], tea leaves [13], sugarcane bagasse [14], and coffee husks [15]. The major compositions of agricultural by-products are lignin and cellulose which include various functional groups such as hydroxyl or phenolic group, aldehydes, ketones and ether linkages [2]. These groups have strong affinities to bind metal ions by electron pair to form complexes. In China, the agricultural waste walnut shell (WNS) is an

*Corresponding author.

abundance biomaterial, which has the above characteristics and can be an alternative adsorbent material. However, raw WNS has low removal capacity for metal ions, and its adsorption efficiency could enhance by grafting functional groups such as carboxyl, hydroxyl and amine [16,17]. The ideal situation is to introduce more than one kind of functional groups at the same time. Therefore, amino acid such as aspartic acid that has both carboxyl and amine groups is a good choice. Amalraj et al. [18] have prepared a new aspartic acid doped polypyrrolevia polymerization of pyrrole with aspartic acid, which showed large adsorption capacity of Cr(VI) as 3.4 mmol/g. Hence, it is possible to modify WNS with aspartic acid to obtain a new adsorbent material with high adsorption capacity.

In this work, two samples (MWNS1 and MWNS2) of new adsorbent were prepared by modified WNS with aspartic acid, and characterized by SEM, elemental analysis, XPS, point of zero charge analysis and N_2–BET analysis. Batch adsorption tests were conducted to investigated the adsorption capacity of Ni(II). Various effects of operation parameters such as adsorbent dosage, pH and temperature on the adsorption capacity were discussed. Kinetic models were used to establish the adsorption kinetic rates. Different isotherm models were tested against the experimental data. The adsorption mechanism of MWNS2 was investigated. Besides, the adsorption thermodynamics was discussed.

2. Experimental

2.1. Reagents and Instruments

Aspartic acid was purchased from Shanghai Yuanju Biotechnology Co., Ltd. Nickel(II) chloride hexahydrate were obtained from Shanghai Macklin Biochemical Co., Ltd. NaOH and ethylene diamine terta acetic acid disodium salt (EDTA) were purchased from Shanghai Lingfeng Chemical Reagent Co. Ltd. HCl (35%) and $NH_3{\cdot}H_2O$ (36%) were obtained from Shanghai Titan Scientific Co., Ltd. Murexide was supplied by Tianjin Fuchen Chemical Reagent Co. Ltd. The chemicals involved were of AR grade. Scanning electron microscope (SEM) was recorded using the Hitachi TM3030 microscope to characterize the WNS before and after modification with aspartic acid. The contents of C, H and N in the samples were measured via a VarioELIII elemental analyzer (ElementarAnalysensysteme GmbH). X-ray photoelectron spectroscopy (XPS) analysis was conducted on an ESCALAB 250Xi photoelectron spectrometer (Thermo Fisher Scientific). The pHs at the point of zero charge (pH_{pzc}) of WNS and MWNS2 were measured in 0.1 mol/L NaCl solution under pH ranging from 2.0 to 12.0, which was adjusted using 0.1 mol/L HCl or 0.1 mol/L NaOH solution on a digital pH meter. The pH_i (initial pH) values and the final pH (pH_f) were accurately noted. The pH_{PZC} was determined from the point of intersection of the plot of the ΔpH *vs.* pH and the x-axis. The Brunauer-Emmett-Teller (BET) were used to measure the surface area by the BET method from N_2 adsorption at 77 K using a high-vacuum volumetric apparatus (mMK-TriStar 3000).

2.2. Modified WNS preparation

WNS, obtained from marketsin Shanghai (China), was smashed and sieved to collect the powders with diameter of 75–150 μm. The powder was washed with distilled water and dried at 80°C until complete dryness. Modified reaction of WNS was carried out as follows: first, the powder of dried WNS (16 g), aspartic acid (29.9 g) and 1.5 mol/L hydrochloric acid solution (150 mL) were mixed with agitation at 90°C for 4 h. Hereafter, the powder was filtered and washed until the eluant was neutral. Afterwards, the washed powders were dried to get the modified WNS named as MWNS1. Then, the MWNS1 (8 g) was dispersed in 200 mL sodium hydroxide solution (1 mol/L) for over 24 h. After that, the powder was filtered, washed with deionized water until the eluant was neutral and dried to obtain the modified WNS marked as MWNS2.

The synthesis route used to prepared MWNS1 and MWNS2 is presented in Fig. 1.

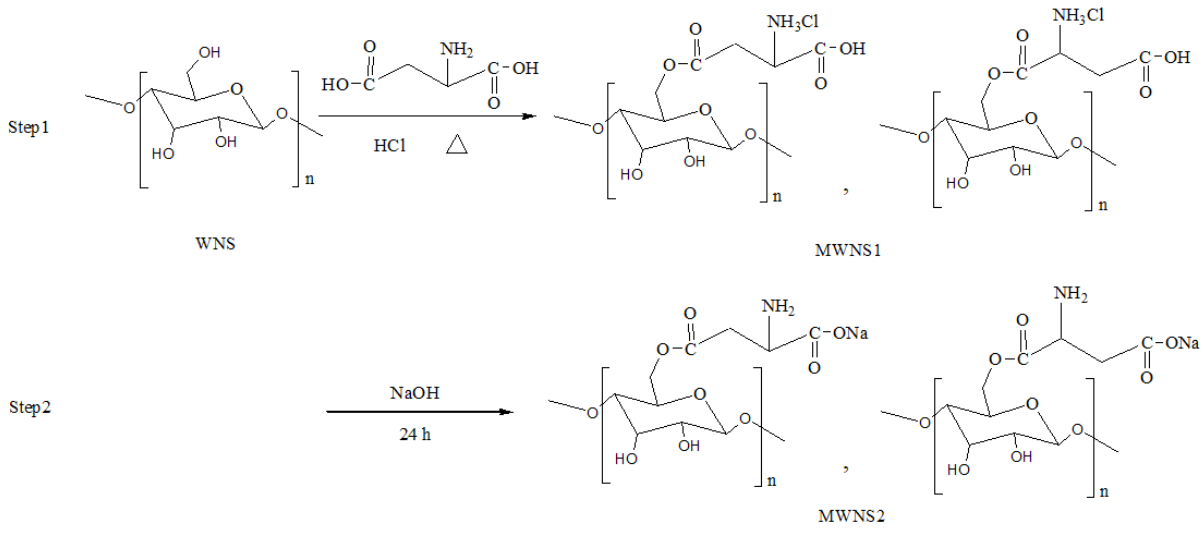

Fig. 1. Synthesis route used to prepare MWNS1 and MWNS2.

2.3. Adsorption experiments

Batch adsorption tests were carried out by mixing a fixed amount of adsorbent with 100 mL nickel ion solution of known concentrations (5.0 mmol/L)in 250 mL stoppered conical flasks, which were put in a thermostated water bath at the set temperature with vigorous shaking until equilibrium achieved. Supernatant solution (2.0 mL) were removed and the Ni(II) concentration was analyzed by EDTA titration. All the tests were performed in duplicate and the mean values were reported with the standard deviations <2%.

The adsorption equilibrium tests were conducted by varying the adsorbent dosage (800–2400 mg/L), pH of initial nickel ion solution (2.0–7.0), different initial nickel ion concentration (0.5–7.0 mmol/L) and temperature (298–318 K). The pH of nickel ion solution was attuned via addition of 0.1 mol/L HCl or NaOH.

The removal efficiency R (%) and equilibrium adsorption capacity q_e (mg/g) were calculated as follows:

$$R(\%) = \frac{(C_0 - C_e)}{C_0} \times 100 \quad (1)$$

$$q_e = \frac{(C_0 - C_e)V}{w} \quad (2)$$

where C_0 and C_e(mg/L) represent the initial and equilibrium concentrations of nickel ion, respectively. V (L) and w (g) are the solution volume and the adsorbent mass, respectively.

The adsorption kinetics experiments were conducted at 298–318 K to determine the equilibrium time from 15 to 600 min. At selected time intervals (15, 30, 45, 60, 90, 120, 180, 240…600 min), 2 mL of sample solution was removed and analysed. The adsorption capacity at time t, q_t (mg/g), was calculated as:

$$q_t = \frac{(C_0 - C_t)V}{w} \quad (3)$$

where C_t(mg/L) is the nickel ion concentration at time t.

2.4. Desorption and regeneration

The recycling property of adsorbent was performed with 1 mol/L $NH_3{\cdot}H_2O$. After adsorption, Ni(II)–loaded adsorbent was filtered, washed with distilled water and then dispersed in 100 mL $NH_3{\cdot}H_2O$ solution. The reused adsorbent was filtered, washed, dried and applied for the next cycle. The adsorption–desorption experiments were executed for four cycles. The regeneration efficiency (W_r) for each cycle could be obtained as follows:

$$W_r(\%) = \frac{q_n}{q_1} \times 100 \quad (4)$$

where q_n and q_1 (mg/g) represent the adsorption capacities for the nth and first cycle, respectively.

3. Results and discussions

3.1. Characterization of WNS, MWNS1 and MWNS2

The SEM images (Fig. 2) demonstrate that the surface morphologies of the MWNS1 and MWNS2 are different from that of WNS. MWNS1 and MWNS2 have more loose porous surface than WNS, indicating MWNS1 and MWNS2 are more favorable for adsorption.

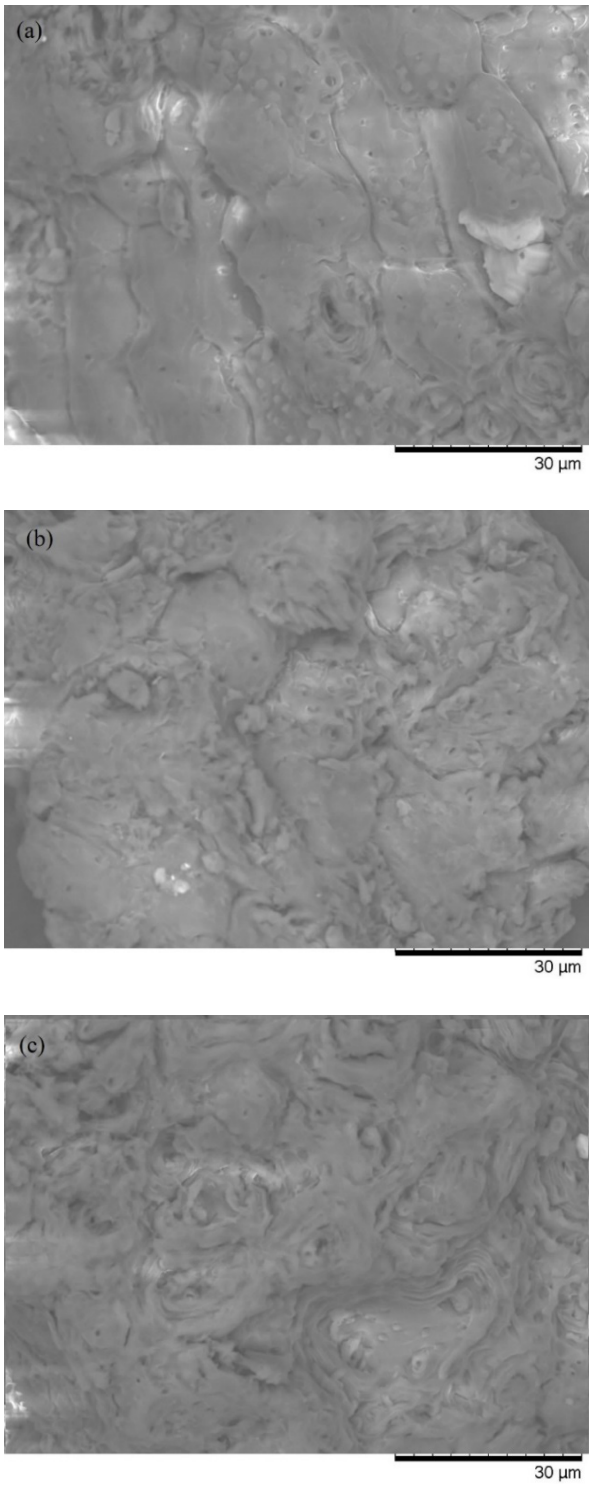

Fig. 2. SEM images of (a) WNS, (b) MWNS1 and (c) MWNS2.

Elemental analysis data of WNS, MWNS1 and MWNS2 presented in Table S1 (available in Supporting Information) show that the proportion of N of MWNS1 and MWNS2

increases compared with WNS, which indicate $–NH_3^+$/$–NH_2$ is successfully grafted to the surface of WNS.

The XPS spectra (WNS and MWNS1) are presented in Fig. 3, and detail analysis of C 1s peak are shown in Table S2. From Fig. 3 and Table S2, the C 1s and N 1s spectra change significantly, and the area ratio for COOH/COOR increase from 2.1% to 8.9%. These results indicate that $–NH_2$ and –COOH, that is aspartic acid, are successfully grafted to the surface of WNS.

The pH_{pzc} and parameters from BET analysis are listed in Table S3. From Table S3, the pH_{pzc} of WNS and MWNS2 does not change much. But the values of surface area, total pore volume and average pore diameter for MWNS2 are all larger than those for WNS, indicating the MWNS2 is more advantageous for adsorption.

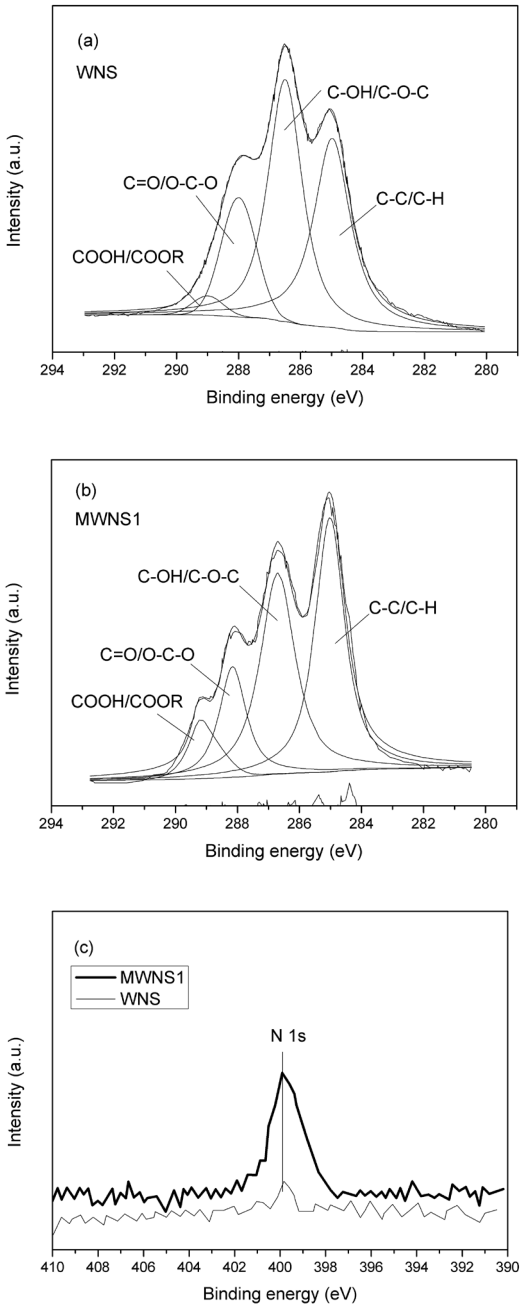

Fig. 3. XPS spectra of (a) WNS (C 1s), (b) MWNS1 (C 1s), (c) N 1s.

3.2. Performance of Nickel ion removal

The relationship between R(%) and t for these three adsorbents (WNS, MWNS1 and MWNS2) is presented in Fig. 4. From Fig. 4, the removal efficiency of WNS for Ni(II) increases gradually until the equilibrium achieved, while the ones of both MWNS1 and MWNS2 increase quickly in the initial stage (60 min), and then the degree of rise clearly decrease until the processes reach to equilibrium. The time to be equilibrium for MWNS1 and MWNS2 (~300 min) is shorter than that for WNS (~360 min). Meanwhile, the removal efficiency of these three adsorbents for Ni(II) ranks in the order of MWNS2 (56.66%) > MWNS1 (43.39%) > WNS (23.22%), which can be explained as follows: as seen in Fig. 1, there are two grafting groups on the surface of MWNS1 ($–NH_3^+$ and –COOH) and MWNS2 ($–NH_2$ and $–COO^-$), respectively. The presence of –COOH, $–COO^-$ and $–NH_2$ could increase the adsorption active sites, and causes higher removal efficiency of Ni(II) than that of WNS. While there is electrostatic repulsion between $–NH_3^+$ and Ni^{2+}, which causes a lower removal efficiency of MWNS1 than that of MWNS2.

3.3. Effect of adsorbent dosage on Ni(II) adsorption

The effect of adsorbent dosage on Ni(II) adsorption onto MWNS2 is shown in Fig. 5. The results indicates that the removal efficiency of Ni(II) increases from 28.33% to 56.66%, whereas the adsorption capacity for Ni(II) is almost a constant as the adsorbent dosage increases from 800 mg/L to 1600 mg/L; after the critical dosage (1600 mg/L), further increase of the dosage has no obvious influence on removal efficiency of Ni(II), but the adsorption capacity decreases. The decrease in Ni(II) uptake at higher adsorbent dosage (>1600 mg/L) may be owing to competition of Ni(II) for

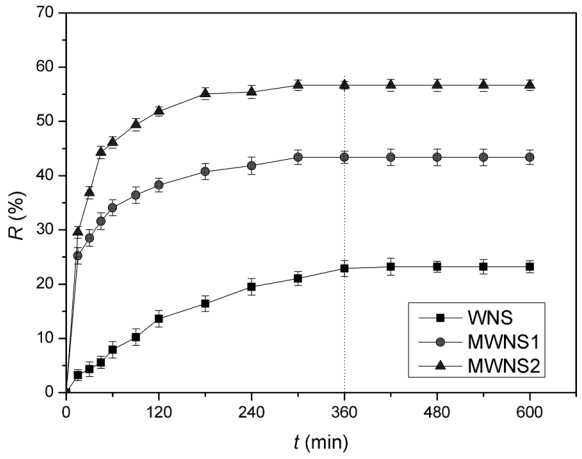

Fig. 4. Nickel ion removal performances of WNS, MWNS1 and MWNS2. (initial nickel ion concentration: 5.0 mmol·L^{-1}; volume of solution: 100 mL; amount of adsorbent: 160 mg; pH: 6.0; temperature: 298 K).

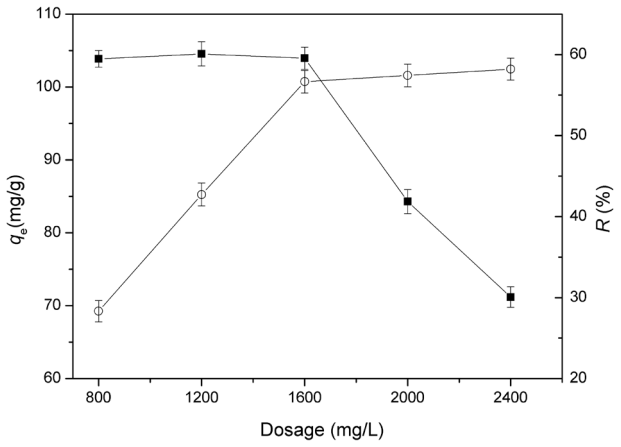

Fig. 5. Effect of adsorbent dose on nickel ion adsorption onto MWNS2. (initial nickel ion concentration: 5.0 mmol·L^{-1}; volume of solution: 100 mL; amount of MWNS2: 80–240 mg; pH: 6.0; temperature: 298 K).

the adsorption sites available [19]. Therefore, 1600 mg/L of adsorbent was selected for later adsorption experiments

3.4. Effect of pH on Ni(II) adsorption

The pH is an crucial factor, which can affect the adsorption of metal ions onto the solid-liquid interface strongly. The effect of pH on the nickel ion removal was studied using 160 mg MWNS2 and Ni(II) solution at 298 K in the pH range 2.0–7.0. Because at pH > 7.52, insoluble nickel hydroxide starts to precipitate from 5.0 mmol/L Ni(II) solution. The results are shown in Fig. 6. As described in Fig. 6, the adsorption capacity increases as the pH of solution increases from 2.0 to 6.0, and then remains constant up to 7.0. At very low pH (pH = 2.0), because –NH_2 will change into –NH_3^+, which means MWNS2 at pH 2.0 will turn into MWNS1 whose adsorption capacity is low. When the pH of solution increase from 2.0 to 6.0, the percentage of –NH_3^+ converted to –NH_2 increases monotonically, which means more and more functional groups (–NH_2) become avail-

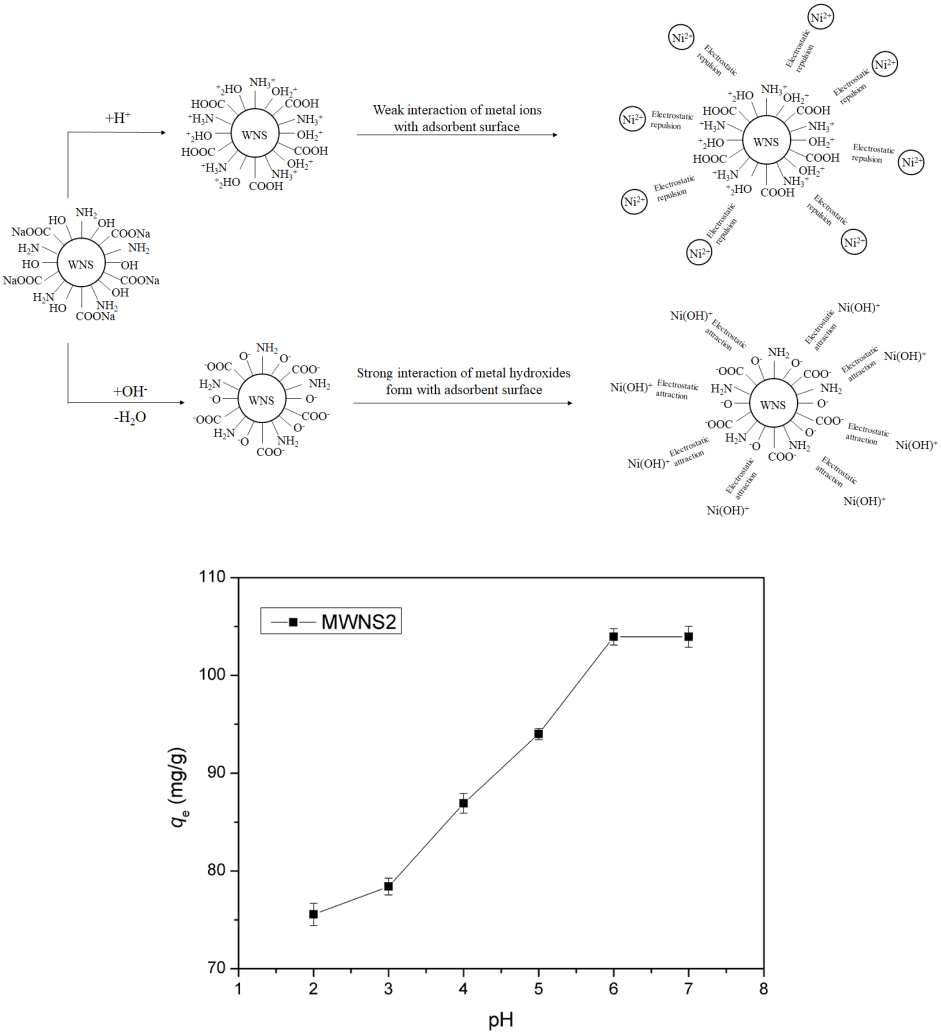

Fig. 6. Effect of pH on nickel ion adsorption onto MWNS2. (initial nickel ion concentration: 5.0 mmol·L^{-1}; volume of solution: 100 mL; amount of MWNS2: 160 mg; pH: 2.0–7.0; temperature: 298 K).

able to increase the degree of complexation between $–NH_2$ and Ni(II) and leads to the increase of adsorption capacity. When the pH increases from 6.0 to 7.0, the adsorption capacity remains a constant, which because a small number of $Ni(OH)_2$ may generate and decrease the interaction between Ni and MWNS2. This could explain the highest adsorption efficiency of MWNS2 at pH 6.0.

3.5. Kinetics

The pseudo-first-order [20], pseudo-second-order [21] and Elovich models [22] are applied to fit the experiment data. The kinetics of Ni(II) adsorption onto adsorbents (WNS, MWNS1 and MWNS2) at 298 K are presented in Fig. S1 (available in Supporting Information).

The pseudo-first-order model is the first rate equation for adsorption in liquid-solid system based on the sorption capacity of solid. The pseudo-second-order model could predict the rate determining step of adsorption process and the bonds nature between the adsorbent and metal ions. The pseudo-first-order and pseudo-second-order models are expressed as follows

$$\ln(q_e - q_t) = \ln q_e - k_1 t \tag{5}$$

$$\frac{t}{q_t} = \frac{1}{k_2 q_e^{\,2}} + \frac{t}{q_e} \tag{6}$$

where k_1 (min^{-1}) and k_2 ($g\,mg^{-1}\,min^{-1}$) represent the pseudo-first-order and pseudo-second-order rate constants, respectively.

The Elovich model was first applied to the chemisorption kinetics of gases on solids [23], but it has been used to describe the adsorption of solutes from a liquid solution in recent years. The Elovich model is written as

$$q_t = \frac{1}{\beta}\ln(\alpha\beta) + \frac{1}{\beta}\ln t \tag{7}$$

where α ($mg\,g^{-1}\,min^{-1}$) and β ($g\,mg^{-1}$) are the initial adsorption rate and the desorption constant, respectively.

The estimated parameter values of the kinetics models and the correlation coefficient (R^2) are listed in Table 1. From Table 1, the R^2 value of the pseudo-first-order for WNS is closer to 1.0. Yet, the R^2 values of the pseudo-second-order for MWNS1 and MWNS2 ($R^2 > 0.999$) are larger than those of the pseudo-first-order model ($R^2 < 0.91$), which reveals that the kinetics of Ni(II) adsorption onto MWNS1 and MWNS2 are represented well with the pseudo-second-order model, and also suggests that the uptake process of Ni(II) by MWNS1 and MWNS2 is the rate-controlling step. Moreover, the R^2 value of the Elovich model for WNS is rather low ($R^2 = 0.9219$), which shows that the Elovich model may not be appropriate to depict the kinetics of Ni(II) adsorption onto WNS. While the Elovich model also fits the kinetic data of Ni(II) adsorption onto MWNS1 and MWNS2 well ($R^2 > 0.97$), indicating the adsorption process is probably related to chemisorption which involves formation of chemical bonds between the metal ions and the function groups on the surface of adsorbents by exchange or share of valence electrons [24]. Further discussion will be conducted in the adsorption isotherms section.

3.6. Effect of temperature on Ni(II) adsorption of MWNS2

The nickel ion removal performances of MWNS2 were investigated in temperature range of 298 to 318 K. The adsorption capacity of MWNS2 for Ni(II) at 298–318 K is presented in Fig. S2. From Fig. S2, with the temperature increased, the adsorption capacity increases and the time to be equilibrium reduces from ~300 min (298 K) to ~180 min (308 K, 318 K). The experimental data are also correlated with the kinetics models as discussed above (Eqs. (5)–(7)), and the estimated parameters are also indicated in Table 1. From Table 1, all the R^2 values (>0.999) of the pseudo-second-order model for MWNS2 at the temperature from 298 to 318 K are more than the ones (<0.91) of the pseudo-first-order model, indicating the experimental data could be represented well with the pseudo-second-order model. Moreover, the adsorption capacity and adsorption rate constant are increased with the increased temperature, which suggests the process of nickel ion adsorption onto MWNS2 is endothermic. Besides, the Elovich model also fits the kinetics data well ($R^2 > 0.97$), indicating the adsorption process is probably related to chemisorption. It is also observed that the values of β for MWNS2 decrease with

Table 1
Kinetic parameters for nickel ion adsorption

Kinetic models		WNS	MWNS1	MWNS2		
	T (K)	298	298	298	308	318
	$q_{e,exp}$ (mg/g)	42.57	79.54	103.87	117.77	130.26
Pseudo-first-order	k_1 (min^{-1})	0.00661	0.04023	0.03757	0.04358	0.04591
	$q_{e,cal}$ (mg/g)	44.84	75.49	101.36	114.85	124.96
	R^2	0.9918	0.7511	0.9088	0.8384	0.7234
Pseudo-second-order	$k_2 \times 10^3$ ($g\,mg^{-1}\,min^{-1}$)	0.1082	0.6406	0.6532	0.6824	0.7122
	$q_{e,cal}$ (mg/g)	56.99	82.23	107.05	120.64	133.77
	R^2	0.9784	0.9997	0.9998	0.9997	0.9997
Elovich	α ($mg\,g^{-1}\,min^{-1}$)	0.8296	47.01	24.41	42.85	67.98
	β ($g\,mg^{-1}$)	0.08126	0.09027	0.05269	0.05013	0.05002
	R^2	0.9219	0.9816	0.9742	0.9908	0.9851

temperatures and the value of α for MWNS2 increase with temperatures due to the endothermic nature. In summary, the increasing temperatures facilitates the process of Ni(II) adsorption onto MWNS2. There are two reasons can explain this trend: first, the increasing temperature promotes the diffusion of the metal ion from bulk solution to bulk adsorbent [25]. Second, the increase in temperature increases the degree of ionization of the function groups, which leads to increase activity of adsorbing metal ions from solution [26].

To analyze the mechanism and rate-controlling steps affecting the adsorption kinetics, intraparticle diffusion equation [17] is applied to fit the kinetic data.

The intraparticle diffusion model is written as

$$q_t = k_{id} t^{0.5} + C \tag{8}$$

where k_{id} (mg g^{-1} min$^{-0.5}$) represents the rate constant of diffusion, C is a coefficient which is proportional to the boundary layer thickness. If the plots of q_t versus $t^{0.5}$ are linear and pass through the origin (C=0), then the rate-controlling step is due only to the intraparticle diffusion [27]. The plots of q_t versus $t^{0.5}$ for the Ni(II) adsorption onto WNS, MWNS1 and MWNS2 at 298 K are depicted in Fig. 7a. The plots of q_t versus $t^{0.5}$ for the Ni(II) adsorption onto MWNS2 at 298–318 K are depicted in Fig. 7b. From Fig. 7, the plots consist of two or three linear portions with different slopes. The multilinearity indicates that two or three steps are operational during the process of Ni(II) adsorption onto WNS, MWNS1 and MWNS2. Besides, the plots don't pass through the origin, which suggests that intraparticle diffusion is one of rate-controlling steps in this adsorption system. From Fig. 7a, the process of Ni(II) adsorption onto WNS at 298 K has two rate-controlling steps including the intraparticle diffusion and the equilibrium plateau, while the ones onto MWNS1 and MWNS2 have three rate-controlling steps including the film diffusion, the intraparticle diffusion and the equilibrium stage. In fact, according to the SEM figures and BET analysis, the porosity and the average pore size of WNS is smaller. So, the effects of intraparticle diffusion are dominant, while the film diffusion is negligible.

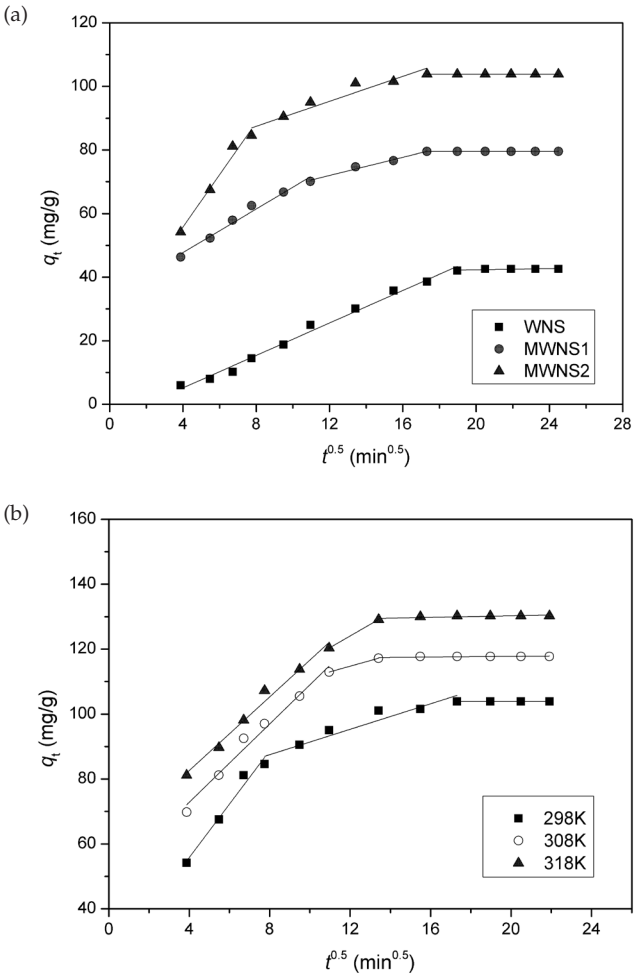

Fig. 7. (a) Plots of q_t *vs* $t^{0.5}$ of nickel ion adsorption onto WNS, MWNS1 and MWNS2 at 298 K. (initial nickel ion concentration: 5.0 mmol·L^{-1}; volume of solution: 100 mL; amount of adsorbent: 160 mg; pH: 6.0); (b) Plots of q_t *vs* $t^{0.5}$ of nickel ion adsorption onto MWNS2. (initial nickel ion concentration: 5.0 mmol·L^{-1}; volume of solution: 100 mL; amount of MWNS2: 160 mg; pH: 6.0; temperature: 298–318 K).

3.7. Adsorption isotherms

The adsorption equilibrium is always fitted by the adsorption isotherms, in which the parameters could indicate the physicochemical property of the adsorbent surface, the adsorbent structure characteristics and the affinity between adsorbate and adsorbent [28]. The equilibrium experimental data are correlated with Langmuir [29], Freundlich [30] and Dubinin–Redushkevich (D–R) models [31].

The Langmuir model assumes that monolayer is formed on the homogeneous adsorbent surface. Langmuir model is

$$\frac{C_e}{q_e} = \frac{C_e}{q_m} + \frac{1}{q_m K_L} \tag{9}$$

where q_m is the maximum monolayer adsorption capacity. K_L is the Langmuir parameter, which is related to the energy of adsorption.

The Freundlich model assumes that the adsorption occurs on the heterogeneous surface with nonuniform adsorption energy. Freundlich model is

$$\ln q_e = \frac{1}{n} \ln C_e + \ln K_F \tag{10}$$

where K_F is the Freundlich constant which can be as an indicator of adsorption capacity, and $1/n$ is the Freundlich parameter related to the adsorption intensity.

The Dubinin–Radushkevich (D–R) model could discriminate between physisorption and chemisorption on both homogenous and heterogeneous surfaces. The D–R model is

$$\ln q_e = \ln q_D - K_D \varepsilon^2 \tag{11}$$

with

$$\varepsilon = RT \ln\left(1 + \frac{1}{C_e}\right) \tag{12}$$

$$E = \frac{1}{\sqrt{2K_D}} \tag{13}$$

where q_D represents the maximum adsorption capacity, K_D is the coefficient related to the adsorption energy. ε is the Polanyi potential and E is the mean energy which is utilized to evaluate the adsorption type. If E < 8.0 kJ/mol, the adsorption process takes place physically; if E > 8 kJ/mol, the adsorption process proceeds chemically [32].

The isotherm data for Ni(II) adsorption onto MWNS2 were obtained at initial nickel ion concentrations ranging from 0.5 to 7.0 mmol/L at 298–318 K. Fig. 8 shows the adsorption equilibrium data (q_e versus C_e) at different temperatures. Fig. 8 suggests that q_e increases with the increase of C_e at a fixed temperature.

3.6.1. Langmuir model

The relationship between C_e/q_e and C_e correlated with the theoretical Eq. (9) at 298–318 K is shown Fig. S3. From Fig. S3, a feature concentration (C_{eL}) exists which is listed in Table 2. For $C_e < C_{eL}$, the plots of C_e/q_e vs. C_e (denoted by solid lines) are linear; while for $C_e > C_{eL}$, the plots of C_e/q_e vs. C_e are denoted by dotted lines. The concentration corresponding to the intersection of the solid and dotted line is defined as the feature concentration. The linear least-squares method was used to obtain the intercepts and slopes. The Langmuir parameters (q_m and K_L) and R^2 are reported in Table 2. The R^2 values of solid lines (0.9903–0.9911) suggest that the experimental data agree closely with Langmuir model at lower nickel ion concentration, indicating that the process is a monolayer adsorption for $C_e < C_{eL}$. When at higher nickel ion concentration, this model is not suitable (R^2 = 0.9085–0.9729) and the adsorption may occur in multilayer fashion for $C_e > C_{eL}$.

3.6.2. Freundlich model

The plots of ln q_e *vs.* ln C_e compared with the theoretical (Eq. (10)) at 298–318 K are shown in Fig. S4. From Fig. S4, a feature concentration (C_{eF}) also exists, and is listed in Table 3. And the Freundlich parameters and R^2 are listed in Table 3. The higher R^2 values (0.9934–0.9990) reveal that the Freundlich model is much better to describe the adsorption process, and there possibly exists the heterogeneity of the surface of MWNS2 for Ni(II) adsorption. Besides, the values of n (0.2032–4.3638) are lower than 10, indicating that this adsorption is a reversible process [33]. From Table 3, the values of K_F and n for $C_e < C_{eF}$ are distinct from the ones for $C_e > C_{eF}$, which suggests that there are two different adsorption mechanisms occurred in these two concentrations ranges, and multilayer adsorption may take place in the higher concentration range. In addition, the n values (0.2032–0.3543) for $C_e > C_{eF}$ are lower, indicating that in this concentration range q_e is more sensitive to C_e.

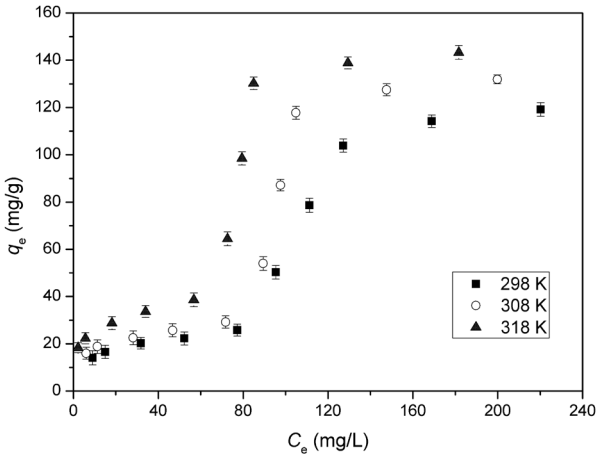

Fig. 8. Adsorption isotherms of nickel ion onto MWNS2 at different temperatures. (initial nickel ion concentration: 0.5–7.0 mmol·L^{-1}; volume of solution: 100 mL; amount of MWNS2: 160 mg; pH: 6.0; temperature: 298–318 K).

3.6.3. D–R Model

The relationship between ln q_e and ε^2 compared with the theoretical (Eqs. (11),(12)) is represented in Fig. S5. From Fig. S5, the plots of ln q_e versus ε^2 consist of two linear portions, that is, there are intersection points ((ε′)^2), which is corresponding to the feature concentrations (C_{eD}). (ε′)^2 and C_{eD} are calculated and reported in Table 4. And the D–R model parameters and R^2 are listed in Table 4. From Table 4, for ε^2 > (ε′)^2($C_e < C_{eD}$), the values of E (13.18–15.99 kJ/mol) are larger than 8 kJ/mol, suggesting chemisorption occurs in this adsorption system. For ε^2 < (ε′)^2($C_e > C_{eD}$), the values of E (2.92–3.90 kJ/mol) are less than 8.0 kJ/mol, suggesting the adsorption belongs to physisorption. These results indicate that the process of Ni(II) adsorption onto MWNS2 is conducted by chemical adsorption for $C_e < C_{eD}$ and followed by physical adsorption for $C_e > C_{eD}$.

From Tables 2, 3 and 4, the mean feature concentration (C_e′) is calculated by

$$C_e' = (C_{eL} + C_{eF} + C_{eD}) / 3 \quad (14)$$

The values of C_e′, relative errors and average deviations for C_{eL}, C_{eF} and C_{eD} are shown in Table 5. The result suggests that the value of C_{eL}, C_{eF} and C_{eD} from the above three models is not much difference between each other with low average deviations (0.0427, 0.0290 and 0.0237). Therefore, the value of C_e′ can be considered as a critical point to distinguish the monolayer chemical adsorption and multilayer physical adsorption. For $C_e < C_e$′, the process of nickel ion adsorption onto MWNS2 is a monolayer chemical adsorption, while at higher concentrations ($C_e > C_e$′), the process is a multilayer physisorption.

The adsorption capacity for Ni(II)contrasted with different adsorbents is shown in Table 6. From Table 6, the adsorption capacity of MWNS2 in this study is three times more than that of untreated WNS. Compared with the adsorption capacity of sodium hydroxide treated rice bran [34] which is 1.32 times more than that of untreated rice bran, indicating modifying WNS with aspartic acid is an ideal method that can effectively increase the adsorption capacity.

3.7. Thermodynamics

The orientation and feasibility of physicochemical adsorption could be estimated by thermodynamic parameters including ΔG, ΔH and ΔS, which can be obtained from follows:

Table 2
Langmuir model parameters for nickel ion adsorption onto MWNS2

		$C_e < C_{eL}$			$C_e > C_{eL}$		
T (K)	C_{eL} (mg/L)	q_m (mg/g)	K_L (L/mg)	R^2	q_m (mg/g)	K_L (L/mg)	R^2
298	72.82	28.75	0.08672	0.9911	–28.41	–0.006403	0.9085
308	71.37	31.59	0.1209	0.9906	–20.00	–0.008211	0.9631
318	60.12	40.72	0.1980	0.9903	–25.58	–0.009895	0.9729

Table 3
Freundlich model parameters for nickel ion adsorption onto MWNS2

		$C_e < C_{eF}$			$C_e > C_{eF}$		
T(K)	C_{eF} (mg/L)	K_F	n	R^2	K_F	n	R^2
298	75.81	7.7928	3.6652	0.9941	1.2558×10^{-4}	0.3543	0.9934
308	78.79	10.4856	4.2432	0.9955	1.3576×10^{-8}	0.2032	0.9945
318	65.01	15.0609	4.3638	0.9982	2.4722×10^{-7}	0.2211	0.9990

Table 4
D–R model parameters for nickel ion adsorption onto MWNS2

			$C_e < C_{eD}$				$C_e > C_{eD}$			
T(K)	$(\varepsilon')^2/10^8$ (J^2/mol^2)	C_{eD} mg/L)	$q_D\times10^4$ (mol/g)	$K_D\times10^9$ (mol^2/J^2)	E (kJ/mol)	R^2	q_D (mol/g)	$K_D\times10^8$ (mol^2/J^2)	E (kJ/mol)	R^2
298	2.7520	72.67	9.37	2.8801	13.18	0.9936	3.63	3.2903	3.90	0.9928
308	2.8693	78.79	9.29	2.2509	14.90	0.9905	4.37	5.8861	2.92	0.9951
318	3.2416	64.82	12.01	1.9557	15.99	0.9918	5.48	4.8940	3.20	0.9992

Table 5
Values of C_e' and relative errors and average deviations for C_{eL}, C_{eF} and C_{eD}

		Relative errors		
T (K)	C_e' (mg/L)	$(C_e' - C_{eL})/C_e'$	$(C_e' - C_{eF})/C_e'$	$(C_e' - C_{eD})/C_e'$
298	73.77	–0.0128	0.0277	–0.0148
308	76.32	–0.0649	0.0324	0.0325
318	63.32	–0.0505	0.0268	0.0237
Average deviations		0.0427	0.0290	0.0237

$$K_c = \frac{C_{es}}{C_e} \tag{15}$$

$$\Delta G = -RT\ln K_c \tag{16}$$

$$\ln K_c = \frac{\Delta S}{R} - \frac{\Delta H}{RT} \tag{17}$$

where K_c is the equilibrium partition constant. C_{es} (mg/g) represents the equilibrium solid-phase concentration. ΔS and ΔH could be obtained from the intercept and slope of the plot of ln K_c versus $1/T$. The negative ΔG at all tested temperatures (–14.90, –15.69 and –16.46 kJ/mol at 298, 308 and 318 K, respectively) indicates the adsorption process of nickel ion onto MWNS2 is thermodynamically favor-

Table 6
Comparison of adsorption capacity of nickel ion onto different adsorbents

Adsorbents	Adsorption capacity (mg/g)	Modifying agent(s)	References
MWNS2	130.26	Aspartic acid and NaOH	This study
MWNS1	79.54	Aspartic acid	This study
WNS	42.57	–	This study
Rice bran	153.6	NaOH	[34]
Rice bran	116.4	–	[34]
Groundnut husk	6.74	Guar Gum	[35]
Moringa oleifera leaves	163.88	NaOH and citric acid	[36]
Oedogonium hatei	44.20	HCl	[37]
Coir pith	38.9	NaOH	[38]
Cashew nut shell	18.87	–	[39]

Table 7
The recycling properties of MWNS2

Cycle number	I	II	III	IV
q (mg/g)	92.51	89.39	87.41	85.70
W_r (%)	89.07	86.06	84.15	82.51

able and spontaneous. The positive ΔH (+24.84 kJ/mol) indicates the adsorption of nickel ion onto MWNS2 is an endothermic process in nature. The positive ΔS (+133.29 J/mol/K) corresponds to an increase in the randomness of the solid-liquid interface during nickel ion adsorption onto MWNS2.

3.8. Verification

To verify the process of Ni(II) adsorption onto MWNS2, the samples before and after adsorption (MWNS2 and nickel–loaded MWNS2) were characterized by EDS, and the EDS images are shown in Fig. S6. From Fig. S6, there is a significant peak for Na(I), while after adsorption, Ni peak emerges and the mass percentage is 9.16%. On the other hand, according to q_e (103.87 mg/g) listed in Table 1, the theoretical mass percentage for nickel-loaded MWNS2 is 9.77%. Thus, the process of Ni(II) adsorption onto MWNS2 and all the results obtained in this study could be acceptable.

3.9. Reusability of MWNS-2

The reusability of adsorbents is another important standard, the results of Ni(II) adsorption onto the recovered MWNS2 after four successive adsorption-desorption cycles are shown in Table 7. As shown in Table 7, the recycled MWNS2 does not show significant decrease in regeneration efficiency (82.51%), and still maintains high adsorption capacity despite four successive cycles. Thus, the MWNS2 can be reused in Ni(II) adsorption.

4. Conclusion

The novel adsorbents (MWNS1 and MWNS2) modified from walnut shell were synthesized and were characterized through SEM, elemental analysis, XPS, point of zero charge analysis and N_2–BET analysis. These adsorbents were applied for the adsorption of Ni(II) from aqueous solution. The effects of various factors such as adsorbent dosage and initial pH on the Ni(II) adsorption were studied, and the optimal conditions in the initial Ni(II) concentration of 5.0 mmol/L solution are 1600 mg/L and pH = 6.0. The adsorption kinetics experiments were performed at 298–318 K. The kinetics of Ni(II) uptake by WNS follow pseudo-first-order model best, while those onto MWNS1 and MWNS2 could agree closely with the pseudo-second-order equation. The Elovich model also fits the kinetic data well for MWNS1 and MWNS2, indicating the adsorption of Ni(II) onto MWNS1 and MWNS2 is related to chemisorption. The results of intraparticle diffusion model suggest that the adsorption of Ni(II) onto MWNS1 and MWNS2 involves intraparticle diffusion, but it is not the only rate-controlling step.

The isotherm data for adsorption of Ni(II) onto MWNS2 were obtained at initial Ni(II) concentrations ranging from 0.5 to 7.0 mmol/L at 298–318 K. the adsorption equilibrium data of Ni(II) onto MWNS2 are correlated with Langmuir, Freundlich and D–R models. Simultaneously, the mean feature concentration (C_e') correlated with temperature is determined. The values of R^2 suggest that the Freundlich model (0.9934–0.9990) is more agreeable than the Langmuir model (0.9085–0.9911). From the above discussion, the adsorption mechanism is described as follows: the process of nickel ion adsorption onto MWNS2 is a monolayer chemical adsorption at lower concentrations ($C_e < C_e'$), while at higher concentrations ($C_e > C_e'$), the process is a multilayer physisorption. The values of thermodynamic parameters (ΔG, ΔH and ΔS) reveal that the process of Ni(II) adsorption onto MWNS2 is thermodynamically favorable, endothermic and entropy driven. The EDS analysis verify that Ni(II) is adsorbed onto MWNS2. What's more, the recovered MWNS2 maintains high regeneration efficiency (82.51%) despite four successive cycles. Based on this research, it can be concluded that MWNS2 can be effectively used for Ni(II) removal from aqueous solution.

Symbols

C_0, C_e, C_t — Concentrations of nickel ion at initial, at equilibrium time and at time t (mg/L)
C_e' — Mean feature concentration (mg/L)
C_{eD} — Feature concentration from D–R model (mg/L)
C_{eF} — Feature concentration from Freundlich model (mg/L)
C_{eL} — Feature concentration from Langmuir model (mg/L)
C_{es} — Equilibrium solid-phase concentration (mg/g)
E — Mean energy of adsorption (kJ/mol)
k_1 — Pseudo-first-order rate constant (min^{-1})
k_2 — Pseudo-second-order rate constant ($g.mg^{-1}.min^{-1}$)
K_c — Equilibrium partition constant
K_D — D–R model coefficient (mol^2/J^2)
K_F — Freundlich constant
k_{id} — Rate constant of diffusion ($mg.g^{-1}.min^{-0.5}$)
K_L — Langmuir parameter (L/mg)
n — Freundlich parameter
q_1,q_n — Adsorption capacities for the first and nth cycle (mg/g)
q_D — Maximum adsorption capacity from D–R model (mg/g)
q_m — Maximum monolayer adsorption capacity (mg/g)
q_t,q_e — Adsorption capacities at time t and at equilibrium time (mg/g)
R — Removal efficiency (%)
T — Absolute temperature (K)
V — Solution volume (L)
w — Adsorbent mass (g)
W_r — Regeneration efficiency (%)
ΔG — Standard Gibbs free energy change (kJ/mol)
ΔH — Enthalpy of reaction (kJ/mol)
ΔS — Entropy of reaction (J/K/mol)

Greek

α — Initial adsorption rate ($mg\,g^{-1}\,min^{-1}$)
β — Desorption constant ($g\,mg^{-1}$)
ε — Polanyi potential (J/mol)

References

[1] N.B. Abbas, M.A. Hossein, G. Mitra, R. Noushin, D. Mahdieh, One-Pot synthesis, characterization and adsorption studies of amine-functionalized magnetite nanoparticles for removal of Cr(VI) and Ni(II) ions from aqueous solution: kinetic, isotherm and thermodynamic studies, J. Environ. Health. Sci., 14 (2016) 11–22.

[2] M.N. Zafar, I. Aslam, R. Nadeem, S. Munir, U.A. Rana, S. Ud-Din Khan, Characterization of chemically modified biosorbents from rice bran for biosorption of Ni(II), J. Taiwan. Ins. Chem. E, 46 (2015) 82–88.

[3] P. Panneerselvam, N. Morad, K.A. Tan, Magnetic nanoparticle (Fe_3O_4) impregnated onto tea waste for the removal of nickel (II) from aqueous solution, J. Hazard. Mater., 186 (2011) 160–168.

[4] B. Volesky, Biosorption of heavy metals. Boca Raton, FL: CRC Press; 1990.

[5] Z.Y. Zhou, D.L. Kong, H.Y. Zhu, N. Wang, Z. Wang, Q. Wang, W. Liu, Q.S. Li, W.D. Zhang, Z.Q. Ren, Preparation and adsorption characteristics of an ion-imprinted polymer for fast removal of Ni(II) ions from aqueous solution, J. Hazard. Mater., 341 (2018) 355–364.

[6] O. Rosskopfová, M. Galamboš, L. Pivarčiová, M. Čaplovičová, P. Rajec, Adsorption of nickel on synthetic hydroxyapatite from aqueous solutions, J. Radioanal. Nucl. Chem., 295 (2013) 459–465.

[7] F. Fu, Q. Wang, Removal of heavy metal ions from wastewaters: A review, J. Environ. Manage., 92 (2011) 407–418.

[8] R.S. Juang, R.C. Shiau, Metal removal from aqueous solutions using chitosan enhanced membrane filtration, J. Membr. Sci., 165 (2000) 159–167.

[9] E. Alemayehu, B. Lennartz, Adsorptive removal of nickel from water using volcanic rocks, Appl. Geochem., 25 (2010) 1596–1602.

[10] E. Pehlivan, T. Altun, Biosorption of chromium (VI) ion from aqueous solutions using walnut, hazelnut and almond shell, J. Hazard. Mater., 155 (2008) 378–384.

[11] S.H. Chen, Q.Y. Yue, B.Y. Gao, X. Xu, Equilibrium and kinetic adsorption study of the adsorptive removal of Cr(VI) using modified wheat residue, J. Colloid. Interf. Sci., 349 (2010) 256–264.

[12] M. Akram, H.N. Bhatti, M. Iqbal, S. Noreen, S. Sadaf, Biocomposite efficiency for Cr(VI) adsorption: Kinetic, equilibrium and thermodynamics studies, J. Environ. Chem. E, 5 (2017) 400–411.

[13] S.S. Ahluwalia, D. Goyal, Removal of heavy metals by waste tea leaves from aqueous solution, Eng. Life. Sci., 5 (2005) 158–162.

[14] O.K. Jr, L.V.A. Gurgel, J.C.P. de Melo, V.R. Botaro, T.M.S. Melo, R.P.F. Gil, L.F. Gil, Adsorption of heavy metal ion from aqueous single metal solution by chemically modified sugarcane bagasse, Biores. Technol., 98 (2007) 1291–1297.

[15] L.S. Oliveira, A.S. Franca, T.M. Alves, S.D. Rocha, Evaluation of untreated coffee husks as potential biosorbents for treatment of dye contaminated waters, J. Hazard. Mater., 155 (2008) 507–512.

[16] L.V.A. Gurgel, R.P. de Freitas, L.F. Gil, Adsorption of Cu(II), Cd(II), and Pb(II) from aqueous single metal solutions by sugarcane bagasse and mercerized sugarcane bagasse chemically modified with succinic anhydride, Carbohyd. Polym., 74 (2008) 922–929.

[17] J.S. Cao, J.X. Lin, F. Fang, M.T. Zhang, Z.R. Hu, A new absorbent by modifying walnut shell for the removal of anionic dye: Kinetic and thermodynamic studies, Biores. Technol., 163 (2014) 199–205.

[18] A. Amalraj, M.K. Selvi, A. Rajeswari, A. Pius, Preparation and characterization of aspartic acid doped polypyrrole for the efficient removal of Cr(VI) from aqueous solution, J. Water. Process. Eng., 11 (2016) 162–173.

[19] S.S. Baral, S.N. Das, G.R. Chaudhury, Y.V. Swamy, P. Rath, Adsorption of Cr(VI) using thermally activated weed Salvinia cucullate, Chem. Eng. J., 139 (2008) 245–255.

[20] S. Lagergren, About the theory of so-called adsorption of soluble substances, Vetenskapsakad. Handl., 24 (1898) 1–9.

[21] Y.S. Ho, G. McKay, Pseudo-second order model for sorption processes, Process. Biochem., 34(5) (1999) 451–465.

[22] A.M. Peers, Elovich adsorption kinetics and the heterogeneous surface, J. Catal., 4 (1965) 499–503.

[23] J. Zeldowitsch, The catalytic oxidation of carbon monoxide on manganese dioxide, Acta. Physicochim. URSS., 1 (1934) 364–449.

[24] M.A. Badawia, N.A. Negmb, M.T.H AbouKanac, H.H. Hefni, M.M. Abdel Moneem, Adsorption of aluminum and lead from wastewater by chitosan-tannic acid modified biopolymers: Isotherms, kinetics, thermodynamics and process mechanism, Int. J. Biol. Macromol., 99 (2017) 465–476.

[25] F. Gode, E. Pehlivan, Adsorption of Cr(III) ions by Turkish brown coals, Fuel. Process. Technol., 86 (2005) 875–884.

[26] Y. Ren, X. Wei, M. Zhang, Adsorption character for removal Cu(II) by magnetic Cu(II) ion impregnated composite adsorbent, J. Hazard. Mater., 158 (2008) 14–22.

[27] J. Huang, X. Wang, X. Deng, Synthesis, characterization, and adsorption properties of phenolic hydroxyl group modified hyper-cross-linked polymeric adsorbent, J. Colloid. Interface Sci., 337 (2009) 19–23.

[28] E.R. Monazam, L.J. Shadle, D.C. Miller, H.W. Pennline, D.J. Fauth, J.S. Hoffman, M.L. Gray, Equilibrium and kinetics analysis of carbon dioxide capture using immobilized amine on a mesoporous silica, AIChE J., 59 (2013) 923–935.

[29] I. Langmuir, Adsorption of gases on plain surfaces of glass-mica and platinum, J. Am. Chem. Soc., 40 (1918) 1361–1403.

[30] H.M.F Freundlic, Uber die adsorption in lusungen, J. Phys. Chem., 57 (1906) 370–385.

[31] M.M. Dubinin, The potential theory of adsorption of gases and vapors for adsorbents with energetically non-uniform surface, Chem. Rev., 60 (1960) 235–266.

[32] A.M. El-Kamash, A.A. Zaki, M.A. El-Geleel, Modeling batch kinetic and thermodynamics of zinc and cadmium ions removal from waste solutions using synthetic zeolite A, J. Hazard. Mater., 127 (2005) 211–220.

[33] N.K. Amin, Removal of direct blue-106 dye from aqueous solution using new activated carbons developed from pomegranate peel: Adsorption equilibrium and kinetics, J. Hazard. Mater., 165 (2009) 52–62.

[34] M.N. Zafar, I. Aslam, R. Nadeem, S. Munir, U.A. Rana, S.U.D. Khan, Characterization of chemically modified biosorbents from rice bran for biosorption of Ni(II), J. Taiwan. Inst. Chem. Eng., 46 (2015) 82–88.

[35] R. Ahmad, S. Haseeb, Absorptive removal of Pb^{2+}, Cu^{2+} and Ni^{2+} from the aqueous solution by using groundnut husk modified with Guar Gum (GG): Kinetic and thermodynamic studies, Groundwater Sustain. Develop., 1 (2015) 41–49.

[36] D.H.K. Reddy, K. Seshaiah, A.V.R. Reddy, S.M. Lee, Optimization of Cd(II), Cu(II) and Ni(II) biosorption by chemically modified Moringa oleifera leaves powder, Carbohydr. Polym., 88 (2012) 1077–1086.

[37] V.K. Gupta, A. Rastogi, A. Nayak, Biosorption of nickel onto treated alga (Oedogoniumhatei): application of isotherm and kinetic models, J. Colloid. Interface. Sci., 342 (2010) 533–539.

[38] A. Ewecharoen, P. Thiravetyan, W. Nakbanpote, Comparison of nickel adsorption from electroplating rinse water by coir pith and modified coir pith, Chem. Eng. J., 137 (2008) 181–188.

[39] P.S. Kumar, S. Ramalingam, S.D. Kirupha, A. Murugesan, T. Vidhyadevi, S. Sivanesan, Adsorption behavior of nickel(II) onto cashew nut shell: equilibrium, thermodynamics, kinetics, mechanism and process design, Chem. Eng. J., 167 (2011) 122–131.

Supporting Information

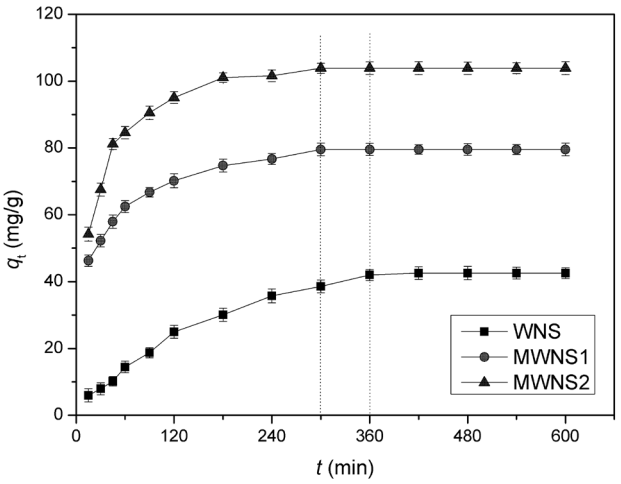

Fig S1. Adsorption kinetics of Ni(II) onto three adsorbents (WNS, MWNS1 and MWNS2) (initial nickel ion concentration: 5.0 mmol·L^{-1}; volume of solution: 100 mL; amount of adsorbent: 160 mg; pH: 6.0; temperature: 298 K).

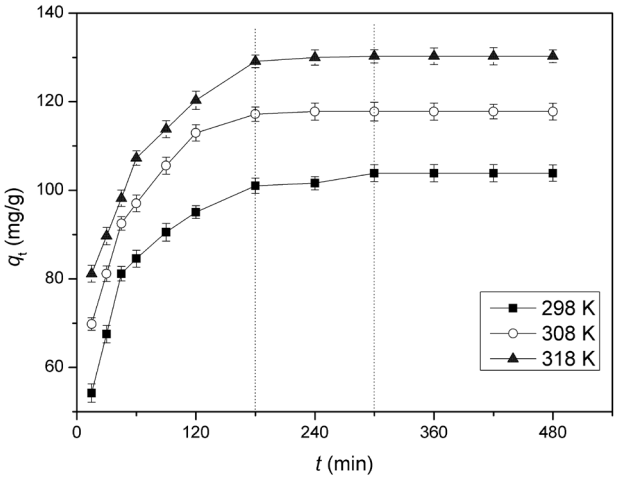

Fig. S2. Effect of temperature on nickel ion adsorption onto MWNS2. (initial nickel ion concentration: 5.0 mmol·L^{-1}; volume of solution: 100 mL; amount of MWNS2: 160 mg; pH: 6.0; temperature: 298–318 K).

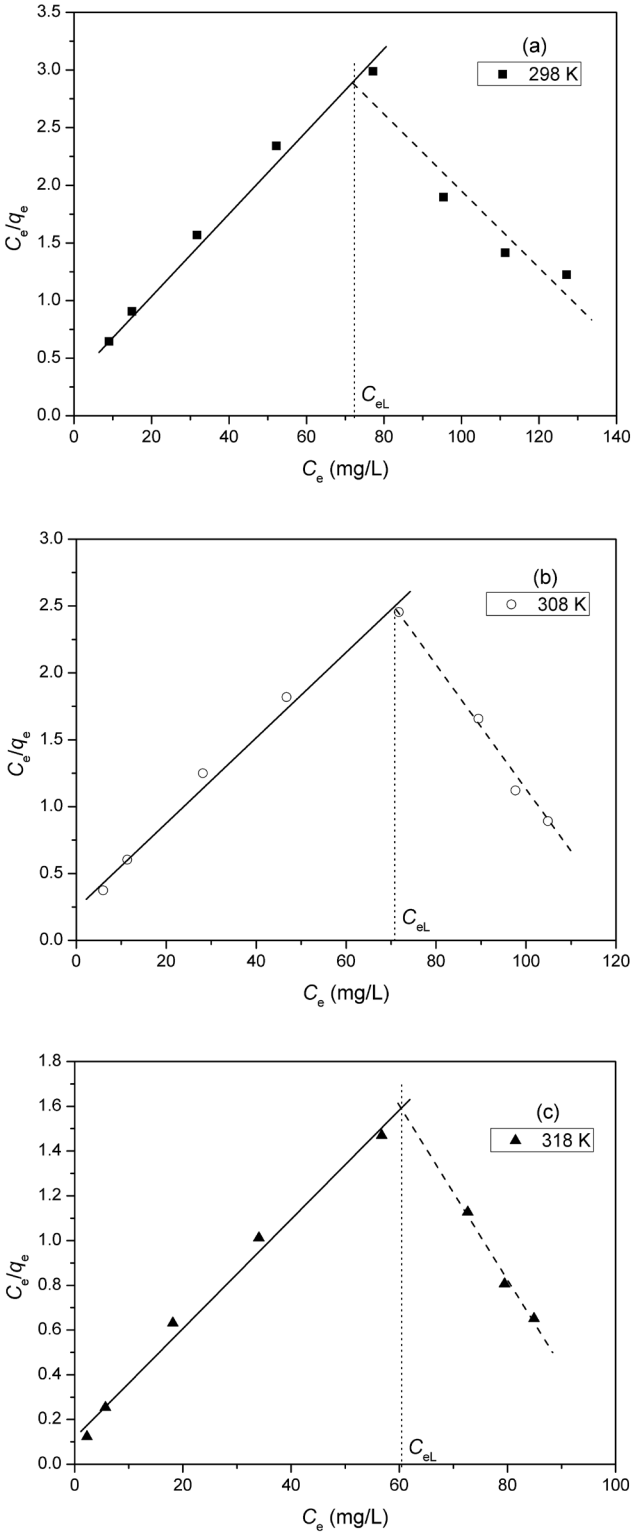

Fig. S3. Langmuir model of nickel ion onto MWNS2 at different temperatures: (a) 298K, (b) 308K, (c) 318K.

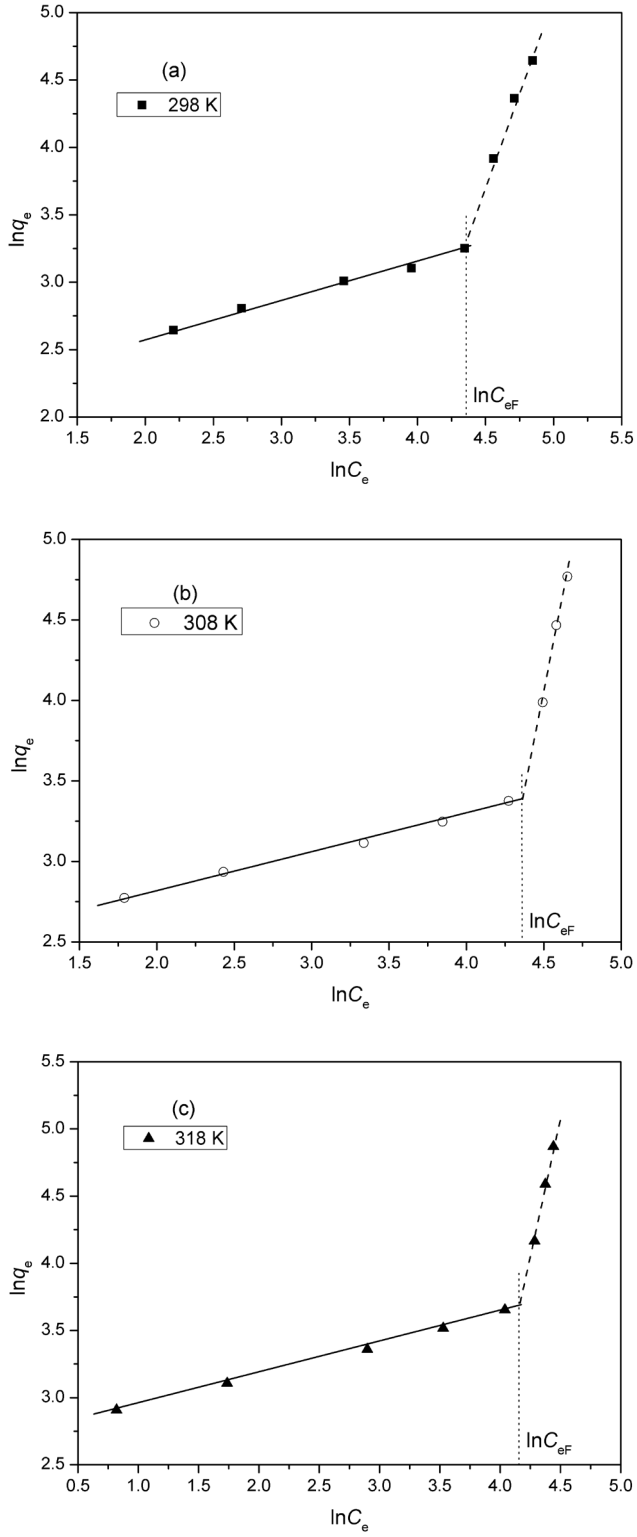

Fig. S4. Freundlich model of nickel ion onto MWNS2 at different temperatures: (a) 298K, (b) 308K, (c) 318K.

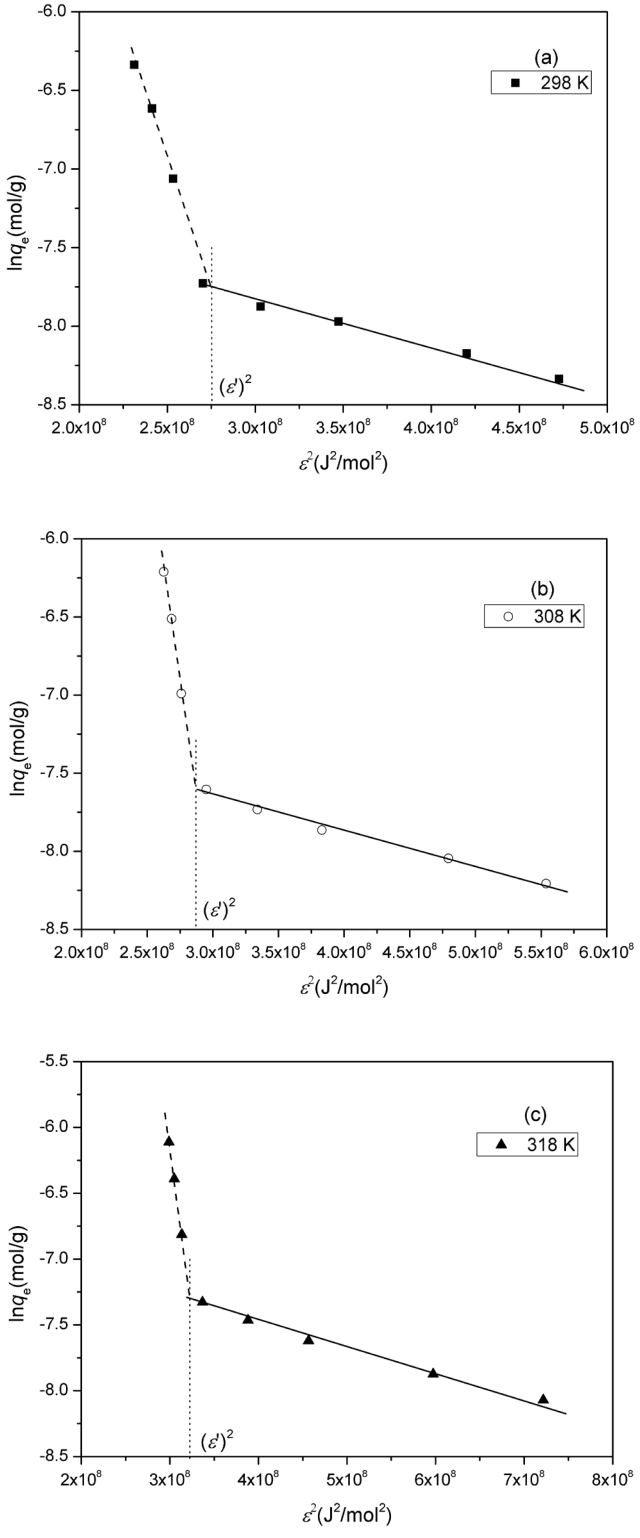

Fig. S5. D-R model of nickel ion onto MWNS2 at different temperatures: (a) 298K, (b) 308K, (c) 318K.

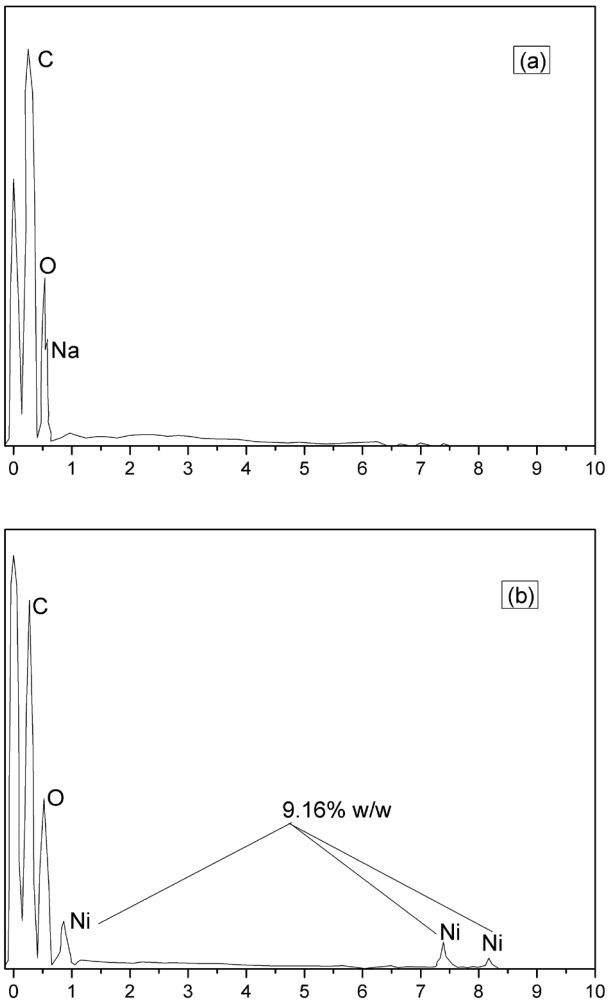

Fig. S6. EDS images of (a) MWNS2 and (b) Nickel-loaded MWNS2.

Table S1
Elemental analysis of WNS, MWNS1 and MWNS2

	C (%)	H (%)	N (%)
WNS	48.82	5.30	0.20
MWNS1	50.39	5.63	1.30
MWNS2	49.85	5.78	1.28

Table S2
Area ratios of C 1s spectra of WNS and MWNS1

Adsorbents	Peak area ratio (%)			
	C-C /C-H	C-OH /C-O-C	C=O /O-C-O	COOH /COOR
WNS	38.2	45.1	14.6	2.1
MWNS1	44.5	34.2	12.4	8.9

Table S3
Characteristics of WNS and MWNS2

Parameters	Value	
	WNS	MWNS2
pH_{pzc}	7.3	7.6
Surface area[a] (m^2/g)	1.04	3.14
Total pore volume[a] ($10^{-3}\,cm^3/g$)	3.13	18.84
Average pore diameter[a] (nm)	12.09	24.01

[a]Determine using N_2–BET analyzer.